doi:10.1016/j.jmb.2004.08.080 J. Mol. Biol. (2004) 343, 1195–1206

JMB

Available online at www.sciencedirect.com

SCIENCE DIRECT®

ELSEVIER

Principles of RNA Compaction: Insights from the Equilibrium Folding Pathway of the P4-P6 RNA Domain in Monovalent Cations

Keiji Takamoto[1,2]†, Rhiju Das[3,4]†, Qin He[1,2], Sebastian Doniach[3] Michael Brenowitz[2,5], Daniel Herschlag[4,6,7]* and Mark R. Chance[1,2,5]*

[1]*Department of Physiology and Biophysics, Albert Einstein College of Medicine of Yeshiva University, New York, NY 10461, USA*

[2]*Center for Synchrotron Bioscience, Albert Einstein College of Medicine of Yeshiva University, New York, NY 10461, USA*

[3]*Department of Physics Stanford University, Stanford CA 94305-4060, USA*

[4]*Department of Biochemistry School of Medicine, Beckman Center, Room B400, Stanford University, Stanford, CA 94305-5307, USA*

[5]*Department of Biochemistry Albert Einstein College of Medicine of Yeshiva University New York, NY 10461, USA*

[6]*Department of Chemistry Stanford University, Stanford CA 94305, USA*

[7]*Biophysics Program, Stanford University, Stanford, CA 94305 USA*

**Corresponding authors*

Counterions are required for RNA folding, and divalent metal ions such as Mg^{2+} are often critical. To dissect the role of counterions, we have compared global and local folding of wild-type and mutant variants of P4-P6 RNA derived from the *Tetrahymena* group I ribozyme in monovalent and in divalent metal ions. A remarkably simple picture of the folding thermodynamics emerges. The equilibrium folding pathway in monovalent ions displays two phases. In the first phase, RNA molecules that are initially in an extended conformation enforced by charge–charge repulsion are relaxed by electrostatic screening to a state with increased flexibility but without formation of long-range tertiary contacts. At higher concentrations of monovalent ions, a state that is nearly identical to the native folded state in the presence of Mg^{2+} is formed, with tertiary contacts that involve base and backbone interactions but without the subset of interactions that involve specific divalent metal ion-binding sites. The folding model derived from these and previous results provides a robust framework for understanding the equilibrium and kinetic folding of RNA.

Keywords: RNA folding; electrostatic relaxation; tertiary interaction formation; compaction; P4–P6 domain

Introduction

The discovery of catalysis by RNA in 1982 by Cech and co-workers engendered excitement on several fronts: an "RNA world" as a potential solution to the evolutionary problem of whether genetic information (nucleic acids) or molecular function (proteins, according to the old view) came first;[1] potential roles for RNA in modern-day biology that extend beyond simply carrying information; and molecular questions of how a polymer far simpler than proteins could fold into discrete three-dimensional structures and direct complex and highly efficient catalysis.[2] Consideration of this

† K.T. & R.D. contributed equally to this work.

Abbreviations used: CE, 10 mM sodium cacodylate, 0.1 mM EDTA buffer; SAXS, small-angle X-ray scattering.

E-mail addresses of the corresponding authors: herschla@cmgm.stanford.edu; mrc@aecom.yu.edu

last problem led to an early focus on the roles of the 2′-hydroxyl group of RNA and of divalent metal ions, both of which were believed to be required for RNA's special functional properties. These views have matured over time.

There are many examples of RNA tertiary structures with intimate roles for 2′-hydroxyl groups, and, indeed, 2′-hydroxyl groups have catalytic roles.[3,4] However, any absolute view of the necessity of the 2′-hydroxyl group for catalysis was vitiated by the discovery, through *in vitro* selection, of DNA catalysts,[5] and these findings were consistent with earlier work showing that DNA of the corresponding sequence can adopt structures similar to tRNA.[6]

Early work with catalytic RNAs demonstrated that addition of divalent metal ions such as Mg^{2+} stimulated RNA structure formation and catalytic activity.[7] One extreme view was that all of RNA catalysis could be reduced to the appropriate placement of catalytic divalent metal ions.[8] However, Co(III) hexammine, an exchange-inert metal ion, or high concentrations of monovalent cations were shown to promote tertiary structure formation for several RNAs,[9–13] and even to promote RNA catalysis in the absence of divalent metal ions.[9,11,14–16] In addition, group I ribozymes were shown to form extensive tertiary contacts at high concentrations of monovalent cations in the absence of divalent cations.[12,13,17] Nevertheless, Mg^{2+} was required to complete the folding of the group I catalytic core required for activity.[13]

To distinguish the factors and forces that control RNA folding, the Na^+-promoted equilibrium folding pathway of the P4-P6 domain of the *Tetrahymena* intron has been dissected. The P4-P6 domain (Figure 1) was chosen for these studies, as its three-dimensional structure is known at atomic resolution with well-defined, specific Mg^{2+}-binding sites[18,19] and its Mg^{2+}-dependent folding has been well-characterized.[20–23] Yet, our initial studies indicated that it collapsed upon addition of monovalent ions alone. Further, this molecule is simple enough, with two regions of long-range tertiary contacts, to allow thorough testing of the roles of these interactions. We have coupled global and local probes with mutagenesis to dissect the behavior of the P4-P6 domain in the presence of monovalent cations. The results, in conjunction with other recent studies, allow us to draw general lessons about the forces that dictate the folding behavior of RNA molecules.

Results

Preformed secondary structure in P4-P6

RNA 'unfolded' states often have stable secondary structure, which simplifies study of folding process. Dimethyl sulfate (DMS) and ribonuclease T1 mapping of the isolated P4-P6 domain verified the presence of intact secondary structure in concentrations of Na^+ as low as 2 mM (data not shown; see also Jaeger *et al.*).[24]

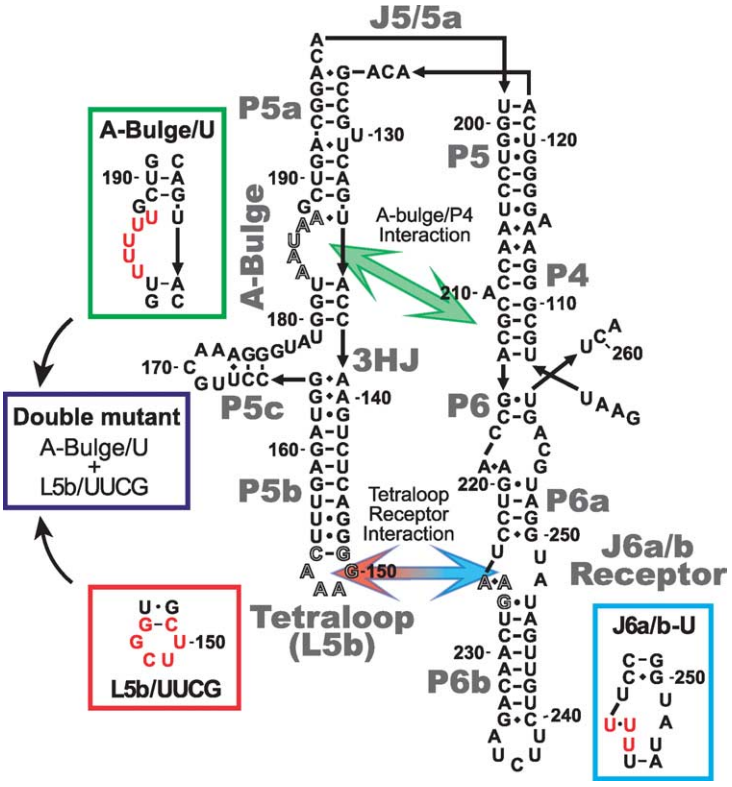

Figure 1. The *Tetrahymena* ribozyme P4-P6 domain and mutants examined in this study. The base-pairing pattern present in the Mg^{2+}-induced native state is shown, and the two long-range tertiary contacts are drawn as arrows. The boxes show the mutant names used and the color coding used in subsequent Figures. The P5abc base-pairing pattern in the absence of Mg^{2+} is likely to be shifted in register by one nucleotide;[47,49] this difference from the native secondary structure does not affect the interpretations or conclusions of this study. Mutation of G174 to A, which favors the non-native secondary structure and destabilizes Mg^{2+}-induced folding,[49] has no detectable effect on the Na^+-induced compaction behavior of P4-P6 (unpublished results).

Two thermodynamic phases of Na^+-induced compaction for P4-P6 RNA

The changes in size of the P4-P6 RNA as a function of the concentration of sodium ions were examined using analytical ultracentrifugation (Figure 2(a)). The hydrodynamic radius, corresponding to the molecule's compactness, decreased in two major phases; the first phase occurs with a midpoint of 10–20 mM Na^+,[21] and the second phase with a midpoint of ~600 mM Na^+. To understand the forces driving these compaction events, we compared the compaction behavior of wild-type P4-P6 RNA to that of a series of mutants. Global information obtained by analytical ultracentrifugation and small-angle X-ray scattering (SAXS) was combined with detailed structural information from hydroxyl radical footprinting to reveal the molecular basis of the compactions.

The first phase: electrostatic relaxation

Despite the reduction in hydrodynamic radius in the first phase of compaction, there are minimal changes in the hydroxyl radical reactivity of the RNA backbone (Figure 2(b)). Thus, the compaction occurs without formation of stable tertiary contacts. To further test for potential roles of tertiary contacts in this phase of compaction, we monitored the size of a mutant form of P4-P6 lacking both long-range tertiary interactions (Figure 1, Double mutant). A transition coincident with that for wild-type RNA was observed (Figure 2(a)), providing additional evidence against the involvement of tertiary interactions in the first phase.

The hydrodynamic radius of 50 Å estimated for the starting state at a very low concentration of Na^+ (<10 mM) is indicative of an extended RNA molecule with the double helical elements splayed away from one another (calculated value 53 Å, *versus* 29 Å for the folded molecule; see Materials and Methods). This extended structure is consistent with charge repulsion determining the orientation of the helices. The results described above suggest strongly that the transition upon increasing the concentration of Na^+ to 100 mM is a structural relaxation that is unaccompanied by formation of tertiary contacts. This relaxation is allowed because of enhanced screening of long-range electrostatic repulsion between the RNA secondary structural elements by the denser Na^+ counterion cloud present at higher concentrations of Na^+.[25] Figure 2(c) shows the distribution of distances between all pairs of atoms within the molecule being probed, $P(R)$, obtained from the SAXS experiments at 100 mM Na^+ and from structural models. The P4-P6 RNA in 100 mM Na^+ is less compact than its native state but considerably more compact than predicted for an extended state. The observed experimental profile is the same as that predicted for a relaxed ensemble of P4-P6 molecules in which electrostatic repulsion is screened but no long-range tertiary interaction is present (Figure 2(c)).

Divalent cations also induce the relaxation. The double mutant RNA examined at 1 mM Mg^{2+} by SAXS has an R_g value and $P(R)$ distribution comparable to that observed at 100 mM Na^+ (Figures 3(a) and 4(a)). Thus, the first phase of compaction reflects an electrostatic relaxation mediated by charge neutralization independent of metal ion valence.

The second phase: compaction induced by tertiary contact formation

At concentrations of Na^+ above 100 mM, further compaction beyond the relaxed state is observed (Figure 2(a)), accompanied by the appearance of protections from hydroxyl radical cleavage (Figure 2(b)). These observations indicate that specific interactions are formed within P4-P6 in the presence of Na^+. This compaction could be mediated through structure formation at the junctions between helices, formation of one or both of the long-range native tertiary contacts or the other non-native tertiary contacts. The observation that the second phase of compaction is absent from a mutant with both long-range tertiary contacts disrupted strongly suggested that one or both of these contacts was responsible for the observed compaction (Figure 2(a)).

To examine the role of the individual tertiary contacts, we investigated P4-P6 constructs with tertiary contacts disrupted separately (Figure 1). Disruption of the tetraloop or its receptor abolished the second phase, whereas disruption of the A-rich bulge had no effect (Figure 4(a)). These results suggested a simple model in which Na^+ supports formation of the tetraloop/tetraloop-receptor but not the contact between the A-rich bulge, which normally binds Mg^{2+}, and its docking site.

The hydroxyl radical cleavage pattern for the wild-type and mutant P4-P6 RNAs provided a further test of the above model as well as a detailed structural comparison to the native state. Remarkably, hydroxyl radical protections for wild-type P4-P6 in high concentrations of Na^+ and in Mg^{2+} were indistinguishable throughout most of its structure, including the "hinge" region between the P4/P5/P6 coaxial stack and P5abc (residues 126–128, 196–97 and 200–202) and the tetraloop/tetraloop-receptor (residues 153–155 and 222–224; Figures 2(b), 4(b) and (c)). Thus, the structure in the presence of a high concentration of Na^+ appears to have the same overall fold as the Mg^{2+} state: parallel neighboring coaxial stacks of P4/P5/P6 and P5abc juxtaposed by the hinge that covalently connects them and the tetraloop/tetraloop-receptor that non-covalently joins these stacks at their distal ends.

Mutation of the tetraloop/tetraloop-receptor prevented the second phase of compaction, as noted above, and abolished protection from hydroxyl radicals (Figure 4(c) *versus* (e); see also

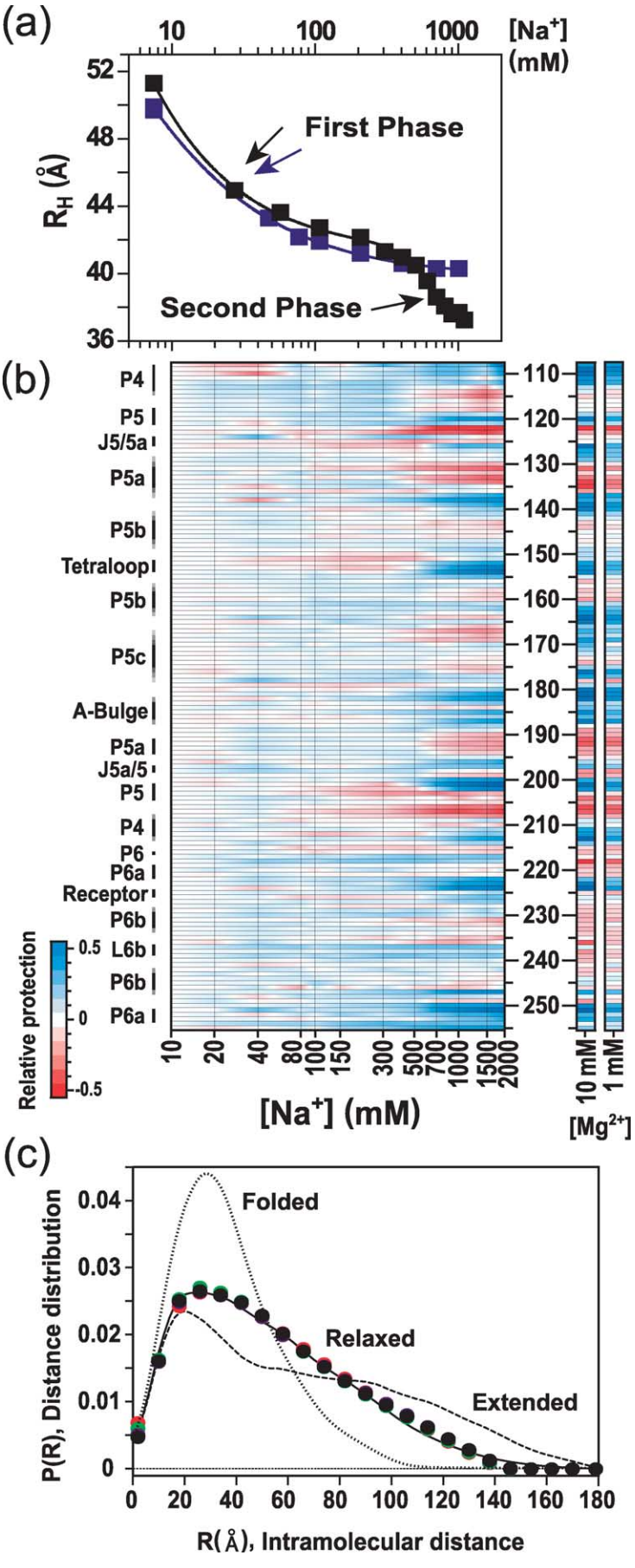

Figure 2. Compaction and tertiary structure formation in the P4-P6 RNA as a function of the concentration of Na^+. (a) P4-P6 compaction, monitored by analytical centrifugation. The hydrodynamic radius for the wild-type P4-P6 (black) is plotted and reveals two thermodynamic phases of compaction, with mid-points of ~20 mM and ~600 mM. The first compaction phase is present in the double mutant (purple). The lines are shown as guides; note the logarithmic scale for the concentration of Na^+. The experimental errors are smaller than the heights of the symbols. (b) Solvent exposure throughout the RNA backbone probed by hydroxyl radical footprinting. Footprinting patterns of the P4-P6 native state in 1 and 10 mM Mg^{2+} are shown for comparison as separate bars at the right. The 10 mM Na^+ state is the reference condition (color white); the Na^+ folding process shows a protection pattern at high concentrations of monovalent ion very similar to that of the native state. Linear interpolation is used to smooth the data between the experimentally measured concentrations of Na^+ to allow better recognition of the transitions in this false-color representation. The measured concentrations are indicated at the bottom of the map. The Na^+ concentration scale matches that in (a) to facilitate comparisons. (c) Small-angle X-ray scattering measurements exhibit indistinguishable distributions $P(R)$ of intramolecular distances R at 100 mM Na^+ for wild-type P4-P6 (black) and variants with mutations disrupting the L5b tetraloop (L5b/UUCG; red), the J6a/b tetraloop receptor (J6a/b-U; cyan), the A-rich-bulge (A-Bulge/U; green), and both the tetraloop and A-rich-bulge (double mutant; purple). Note that overlap obscures most of the data points. The $P(R)$ distribution measured at 100 mM Na^+ is consistent with a relaxed ensemble of P4-P6 conformations (continuous line), but not a highly extended state (dashed line) or the native state (dotted line).

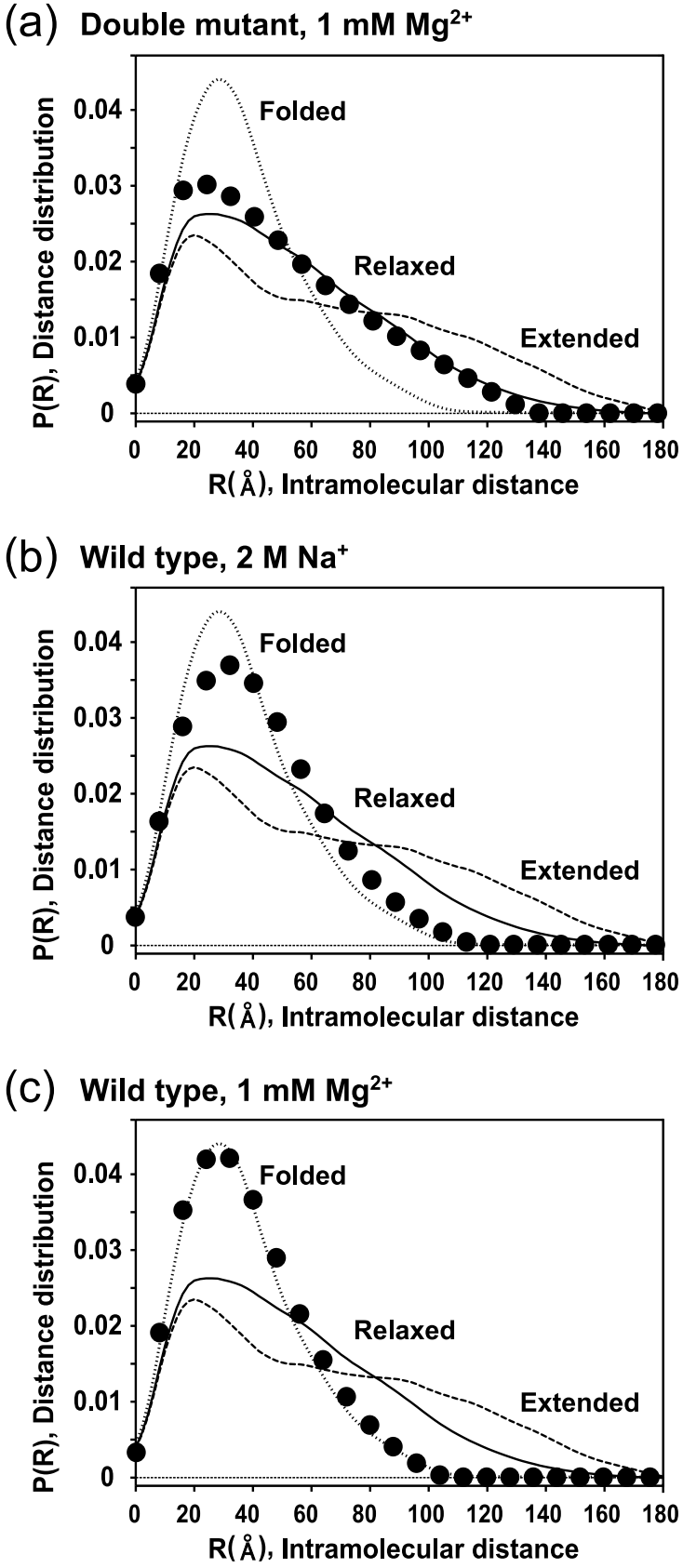

Figure 3. Intermolecular distance distributions of the P4-P6 RNA states discussed in the main text. Symbols show experimental distributions overlaid on predictions for extended, relaxed, and folded (native) states. (a) The double mutant (A-rich/U; L5b/UUCG) is relaxed but not folded in 1 mM Mg^{2+}. (b) The wild-type RNA in high Na^{+} is compact but not native. (c) The wild-type RNA in 1 mM Mg^{2+} forms a conformation whose distance distribution is consistent with the native structure, as expected. The experimental errors are smaller than the heights of the symbols.

Supplementary Material, Figure S1). This result provides additional evidence that the tetraloop/ tetraloop-receptor interaction is formed and is required to stabilize the folded state in Na^{+}. Conversely, mutation of the A-rich bulge, which had no effect on Na^{+}-induced compaction, also had no effect on the protection pattern (Figure 4(c) *versus* (d)).

The above results are consistent with the

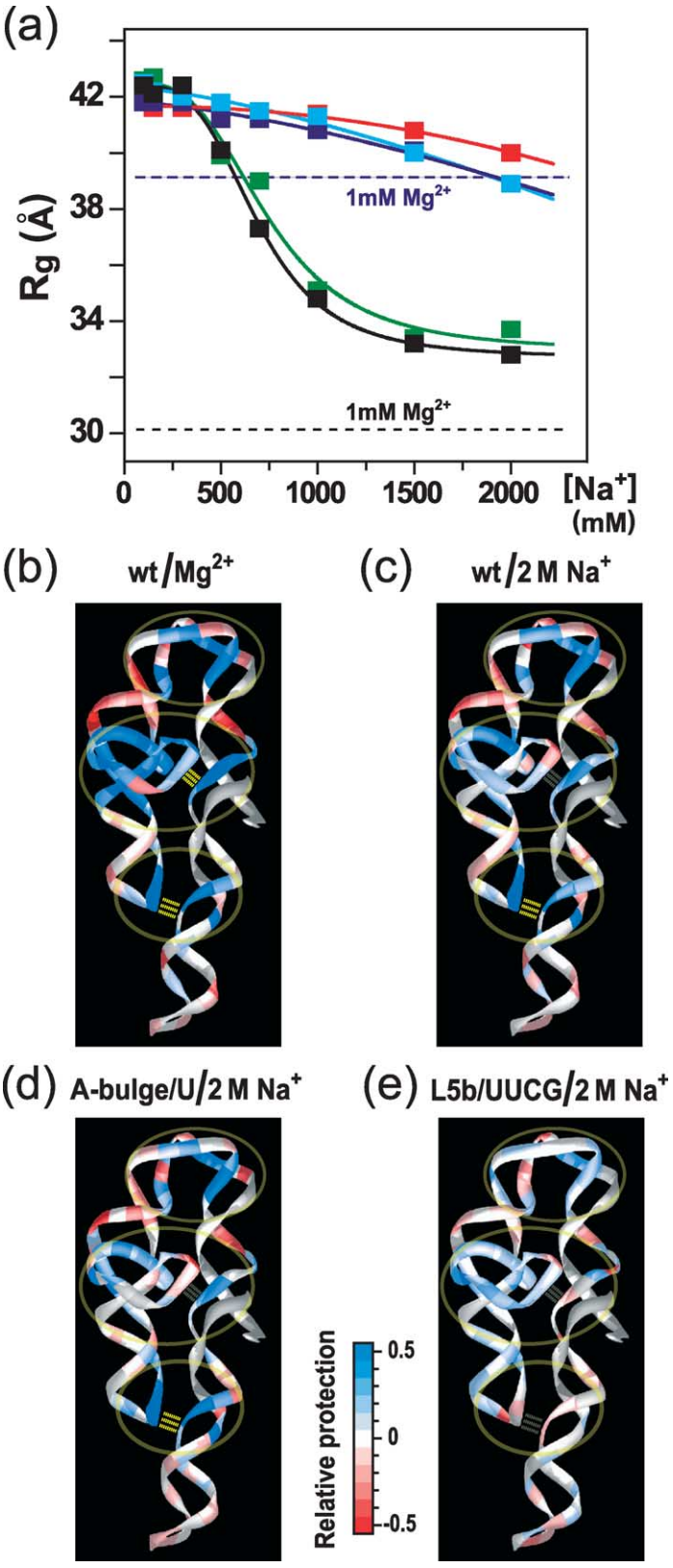

Figure 4. Dissecting the second phase of Na^+-induced compaction of the P4-P6 domain. (a) SAXS measurements of the radius of gyration for the wild-type (black), L5b/UUCG (red), J6a/b-U (cyan), A-Bulge/U (green), and double mutant (purple) molecules. Dashed lines represent the radius of gyration values of wild-type P4-P6 (black) and the double mutant (purple) in 1 mM Mg^{2+}. Radius of gyration values in 1 mM Mg^{2+} for the L5b/UUCG (41 Å), J6a/b-U (39 Å), and A-Bulge/U (41 Å) molecules were within error of the double mutant value (39 Å). (b)–(e) Hydroxyl radical protection pattern of wild-type P4-P6 in (b) 10 mM Mg^{2+}, (c) wild-type in 2 M Na^+, (d) A-Bulge/U mutant in 2 M Na^+, and (e) L5b/UUCG mutant in 2 M Na^+. Protections are relative to reactivity in 10 mM sodium cacodylate buffer in the absence of Mg^{2+}. For visual comparison, the protection patterns for the states are all displayed as color variations on the same backbone representation of the P4-P6 native fold in Mg^{2+}, although conformational differences are indicated by the different protection patterns. The bright or faint gold lines represent the interpreted presence or absence of the tertiary contacts, respectively.

involvement of Mg^{2+} in establishing the structure of the A-rich bulge in the native state and contributing to folding in Mg^{2+} but not in Na^+. As expected, protections surrounding the Mg^{2+} core and in its P4 docking site were diminished greatly in the presence of Na^+ compared to Mg^{2+} (residues 162–165, 169–170, 176–177, 211–214 in Figures 2(b), 4(b) and (c)). The protection pattern for this high-Na^+, near-native state indicates a tertiary structure similar to that of the A-bulge/U mutant folded either by Na^+ or Mg^{2+} (see also Supplementary Material, Figure S2).

In summary, high concentrations of Na^+ alone support folding to a P4-P6 structure that is the same in nearly all respects as the native fold promoted by Mg^{2+}. Structural elements at the ends of the coaxially stacked structural elements, the "hinge" region and the tetraloop/tetraloop-receptor, form in Na^+, whereas interactions mediated by the A-rich bulge that is directly involved in Mg^{2+}-binding are not present.

Discussion

Mg^{2+} and RNA have long enjoyed a special relationship. Mg^{2+} is ubiquitous in physiological environments, and there are clear roles for Mg^{2+} in RNA structure and function. Nevertheless, it has become increasingly clear that RNA can adopt native structure and carry out function in decidedly non-physiological ionic conditions: at high concentrations of monovalent ions in the absence of Mg^{2+}.[9–15] Fundamental insights can be achieved by determining the effects of perturbations away from physiological conditions and dissecting the underlying causes of these effects. Here, we have dissected the equilibrium folding pathway for the P4-P6 RNA domain from the *Tetrahymena* group I ribozyme in monovalent cations using global and local structural probes in conjunction with targeted mutagenesis (Figure 5). Comparing these results with published studies of the structure and folding of this RNA in the presence of Mg^{2+} allows an incisive evaluation of the forces and features proposed to contribute to RNA folding.

RNA "collapse" preceding tertiary structure formation

Secondary structure formation

A simplifying feature of RNA folding, in comparison to protein folding, is the ability to form "unfolded" states with stable secondary structure and to then follow the adoption of compact tertiary structures by these preformed helices. Compact intermediates have been observed in the extensive studies of the kinetic and thermodynamic folding pathways of several RNAs.[17,26–29,57] For the RNase P RNA, *Azoarcus* and bI5 group I introns, the observed thermodynamic compaction with increasing concentration of Mg^{2+} appears to involve, at least in part, secondary structure formation beyond the extensive local duplex formation present in the starting state.[28,30,31] In contrast, DMS and RNase T1 mapping of the P4-P6 domain in the presence of sodium ion concentrations as low as 2 mM suggest that the secondary structure is preformed, simplifying evaluation of other compaction forces.

In addition to inducing a net compaction in the RNA, secondary structure formation greatly constrains the RNA conformational ensemble, and these constraints generally favor formation of native tertiary interactions and disfavor formation of many potential non-native secondary and tertiary interactions.[32] Although this contribution to folding was not probed directly in this study, the preformed secondary structure is undoubtedly a critical feature in favoring subsequent P4-P6 RNA tertiary structure formation.

Electrostatic relaxation

Our equilibrium study, like much of the literature probing the kinetics and thermodynamics of metal ion-dependent RNA folding, used an initial state with very little salt present. For P4-P6 and the complete *Tetrahymena* ribozyme, electrostatic repulsion dominates the interactions between the preformed secondary structural elements at low ionic strength, forcing them into an extended structure (Figure 5(a)).[12,33] Upon the addition of

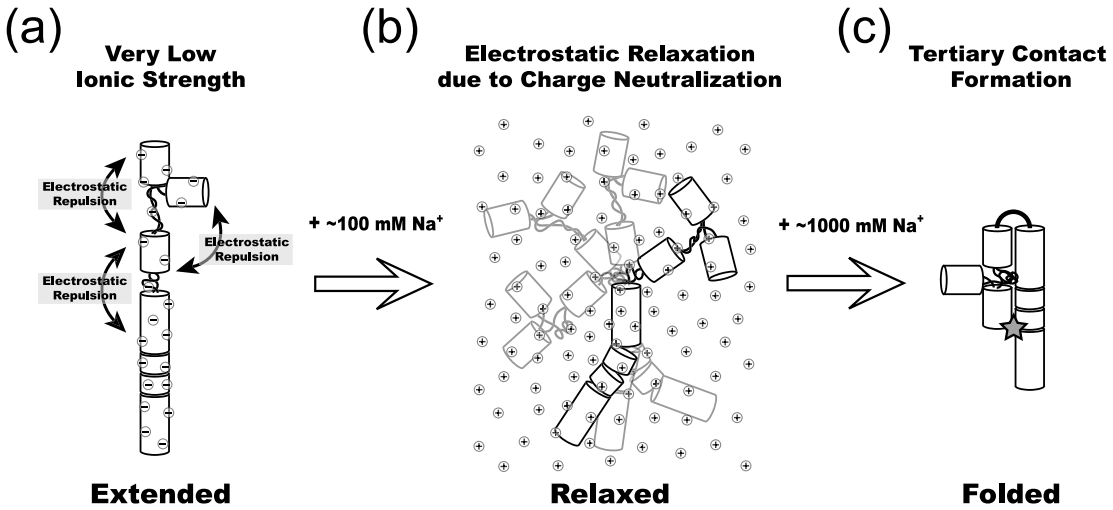

Figure 5. Proposed structural ensembles of the *Tetrahymena* ribozyme P4-P6 domain with increasing concentrations of Na^+.

cations sufficient to neutralize the charge repulsion, the RNA relaxes into a disordered family of structures in which the helices sample alternative conformations that allow tertiary elements to encounter each other (Figure 5(b); see also refs[33,51,52]). This sampling yields a net observed "collapse" as the average molecular radius is decreased. However, the number of accessible conformations is predicted to increase *via* this relaxation process, and this prediction may be testable by thermodynamic and biophysical probes of the conformational flexibility of RNA.[53–55] Electrostatic relaxation is an overall property of the P4-P6 structure in which the rigid charged helices are interconnected by multiple unpaired junctions, and this relaxation is likely to be a general property of the kinetics and thermodynamics of nucleic acids. Indeed, we expect that unstructured states *in vivo* will be electrostatically relaxed rather than dominated by electrostatic repulsion as observed in the low-salt conditions used in many *in vitro* folding experiments.

Counterion-induced attraction

The theories of the counterion atmosphere surrounding nucleic acids provide possible mechanisms of compaction beyond electrostatic relaxation.[34,35] Simulations of the ion atmosphere indicate the existence of a counterion-mediated attractive force between nucleic acid elements and suggest strongly that only counterions of high valence can establish such a force.[35] The observation of compaction of the P4-P6 RNA in the presence of both Na^+ and Mg^{2+} (Figures 2(a) and 3) provides no indication of a valence-dependent counterion correlation force playing a major role in RNA folding.[33]

Tertiary structure formation

Long-range tertiary contacts and specific metal ion-binding sites

The group I introns from *Tetrahymena* and *Azoarcus* can fold into compact, near-native three-dimensional structures in the presence of high concentrations of monovalent ions, although the addition of Mg^{2+} is required for proper folding of the conserved intron catalytic core.[12,13] From these studies it remained unclear whether Na^+ alone could induce significant folding of the isolated P4-P6 domain. In particular, the Mg^{2+} cluster at the core of the P4-P6 RNA[19] was expected to become more important and possibly critical for the domain's folding outside the context of the multiple other ribozyme elements that encapsulate and stabilize the domain.[56] We observe here a compaction of the isolated P4-P6 to nearly native dimensions upon addition of high concentrations of Na^+, demonstrating that its metal ion core is not essential for formation of a compact fold.

The structure of the folded P4-P6 RNA in the presence of a high concentration of Na^+ can be understood from the simplest perspective of the potential effects of monovalent cations. More generally, all RNAs will experience enormous internal electrostatic repulsion between backbone phosphate groups. As described above, moderate concentrations of Na^+ can provide the non-specific electrostatic screening required for relaxation; higher concentrations of Na^+ can then screen charge repulsion of phosphoryl oxygen atoms at the close separations observed in the native fold. With sufficient screening, structural interactions that do not rely on binding of divalent metal ions in specific sites can be formed to give the specific tertiary fold. Although folding of the special tertiary motifs that require Mg^{2+} coordination is not required to form a compact fold, such metal ion-binding sites can provide added stability to folded structures when divalent metal ions are present. Monovalent ions can also stabilize the fold due to the presence of specific binding sites, such as the one identified adjacent to the tetraloop receptor of P4-P6.[36,37]

Local structure at junctions

The importance of structure formation at junctions between double helices for RNA folding has been increasingly recognized.[38,39] For the P4-P6 RNA, mutants with changes within the junction connecting the P4/P5/P6 stack to the P5abc stack (Figure 1) require higher concentrations of Mg^{2+} to fold.[40] This junction also exhibits protections from hydroxyl radical cleavage in the folded state,[20] and these protections are maintained in the Na^+-folded state (Figures 2(b), and 4(b) and (c)).

Beyond their thermodynamic importance in stabilizing RNA folds, junctions may play key roles in folding kinetics.[38] In the case of the P4-P6 RNA, formation of specific tertiary contacts occurs with an observed rate constant of 1–2 s^{-1} when Mg^{2+}-dependent folding is initiated from a low-salt condition (<10 mM); increasing the initial concentration of monovalent ions to 20–30 mM increases the rate of folding at least 25-fold.[21,22,41] The thermodynamic transition from an extended state to a relaxed state with a Na^+ midpoint of ~10 mM could account for this dramatic acceleration, with relaxation of the junctions in the extended state providing one of the kinetic barriers to folding at low concentrations of salt (Figure 5).

The slow folding of junctions may arise due to structure formation that needs to be disrupted. The low-salt P4-P6 structure exhibits no change in the backbone protection pattern of the extended and relaxed states (Figure 2(b)) and may involve stacking of bases at the junctions. A similar kinetic barrier arising from junction structure has been proposed for electrostatic relaxation in the full-length ribozyme based on time-resolved SAXS studies.[33] More generally, structures formed at junctions can aid or hinder folding kinetics and thermodynamics, despite the typical focus in folding on the residues that make specific long-range interactions.

A general picture for RNA folding: a balance of forces

The forces and features described in the preceding sections balance to provide the thermodynamic and kinetic pathways observed for RNA folding. Positioning *via* secondary structure formation, screening of electrostatic repulsion, long-range tertiary interactions, junction structures and specific metal ion-binding sites all play important roles in the formation of a compact, stable P4-P6 RNA. Their balance leads to cooperative folding from an extended, unfolded state to the native state with increasing concentrations of Mg^{2+}. In the absence of Mg^{2+}, binding sites for divalent metal ions no longer play a role, and the balance of the forces shifts, revealing two additional states of P4-P6 (Figure 5). As the concentration of Na^+ is increased, the RNA first compacts to an electrostatically relaxed state and then adopts a near-native tertiary structure lacking the metal ion core but stabilized by Mg^{2+}-independent tertiary interactions. These states are normally hidden in the Mg^{2+} equilibrium folding pathway, but have been revealed in the presence of Mg^{2+} through the appropriate mutations of metal ion-binding sites and long-range contacts.

The ability to fold RNAs in the presence of monovalent ions provides an analytical tool that will aid in developing a complete quantitative energetic description of the forces that dictate RNA structure and dynamics. Such a description is foundational, in turn, for developing a deep understanding of the thermodynamic and kinetic mechanisms underlying the function of RNA molecules involved in complex biological processes.

Materials and Methods

RNA preparation

Wild-type and mutant P4-P6 RNA constructs were prepared by *in vitro* transcription from PCR-generated DNA templates using phage T7 RNA polymerase, labeled at the 5′-end with [γ-^{32}P]ATP using phage T4 polynucleotide kinase for footprinting experiments, and purified by denaturing polyacrylamide gel electrophoresis.

Analytical ultracentrifugation

The RNA stock solutions in CE buffer (10 mM sodium cacodylate, 0.1 mM EDTA, pH 7.0) were diluted into CE buffer containing the indicated concentration of NaCl, heated to 95 °C for one minute, cooled on the bench for 30 seconds and then incubated at 50 °C for 15–30 minutes prior to loading the centrifuge cells. The loaded cells and rotor were allowed to temperature-equilibrate for ~30 minutes in the centrifuge prior to initiating a run. Sedimentation velocity analyses were conducted using the absorption optics of a Beckman XL-I analytical ultracentrifuge at 25 °C, 6 μg/ml of RNA in double-sector cells loaded into a Ti-60 rotor at a rotor speed of 40,000 rpm. The sedimentation boundaries were analyzed as described, assuming $\bar{\nu} = 0.53$ cm^3/g.[12,21] The sedimentation and diffusion coefficients decrease with increasing concentration of Na^+, consistent with compaction of the RNA. The presence of 0.1 mM EDTA in the ultracentrifuge experiments ensures that micromolar multivalent metal ion contaminants potentially associated with NaCl stocks are not responsible for the observed transitions.

Hydroxyl radical footprinting

Radiolabeled RNA samples were denatured at 95 °C for one minute in CE buffer and then incubated at various concentrations of salt at 25 °C for 30 minutes. Fenton chemistry was carried out for 30 minutes at 25 °C with final concentrations of 2 mM $Fe(NH_4)_2(SO_4)_2$, 2.5 mM EDTA, and 6 mM sodium ascorbate without H_2O_2. The reaction products were processed, separated by gel electrophoresis and visualized using phosphor storage imaging.[12,23] The resulting monovalent cation titration autoradiograms were analyzed with single-nucleotide resolution.[12,50] The reactivity data are presented as a false-color image following scaling to reference state, as follows:[12]

$$\text{Relative protection} = 1 - \frac{R}{R_{\text{ref}}}$$

where R is the observed intensity and R_{ref} is the intensity for the initial state in CE buffer. Footprinting of the low-sodium and high-sodium states of the wild-type and A-Bulge/U constructs at independent laboratories with independently purified RNA led to indistinguishable results. As in the ultracentrifuge experiments, the presence of excess EDTA would serve to scavenge micromolar multivalent metal ion contaminants that might be present in the NaCl stocks.

Small-angle X-ray scattering (SAXS)

SAXS samples contained RNA concentrations of 1 or 3 mg/ml of RNA or no RNA (for background measurements) with 50 mM sodium 3-(*N*-morpholino) propanesulfonic acid, pH 7.0 (20 mM Na^+) and various concentrations of sodium acetate. The reported SAXS profiles exhibited no dependence on RNA concentration, indicating that aggregation is negligible. While no EDTA was present in the SAXS experiments, the high concentration of phosphate (>2 mM) of negatively charged RNA ensures that the micromolar levels of multivalent ion contaminants that could be present in the sodium acetate would be insufficient to influence a majority of the RNA molecules present; the agreement in the dependence of the ultracentrifuge results on the concentration of Na^+, for which EDTA was present, and the SAXS results provides further strong evidence against an effect from contaminating multivalent metal ions. Charged coupling device (CCD) images were obtained at beamline 15-A at the Photon Factory and beamline 12-ID at the Advanced Photon Source and processed into SAXS profiles using standard software packages.[42,43] Complete Na^+ titrations of the wild-type and A-Bulge/U constructs were carried out at both beamlines with independently prepared RNA samples and agreed within measurement error. Distance distributions and radius-of-gyration (R_g) values were obtained from SAXS profiles by Svergun's regularized transformation.[44] The resulting R_g values were indistinguishable from those obtained by Guinier analysis. SAXS profiles at low concentrations of Na^+ (<100 mM) could not be used to obtain radii of gyration

or intramolecular distance distributions because of an RNA concentration-dependent scattering signal from intermolecular ordering. In fact, this ordering is a qualitative indicator of strong intermolecular Coulombic repulsion, consistent with strong intramolecular repulsion proposed for the RNA extended state under these conditions.[45] Under all other conditions, the observed scattering was independent of RNA concentration.

Theoretical SAXS distributions and radius of gyration (R_g) values for different RNA conformations, taking into account ion atmosphere scattering effects,[46] were simulated in Matlab routines. The native state structure was taken from PDB coordinates 1GID,[18] with $R_g = 29$ Å. The extended state was taken to be a conformation with the orientation of P5abc adjusted to be at a maximal distance from the stacked P4/P5/P6 helices, corresponding to a maximum radius of gyration of 53 Å. The relaxed ensemble was simulated by uniformly sampling orientations of the P5abc subdomain relative to the P4/P5/P6 helices, yielding an intermediate radius of gyration value, $R_g = 43$ Å. Shifting the base-pairing pattern of P5abc[47] or introducing flexibility at the P5abc and P4/P6 junctions produced no distinguishable changes in the predicted distribution for the relaxed state at the coarse resolution sampled by SAXS.

DMS and RNase T_1 structure mapping

Dimethyl sulfate (DMS) footprinting was carried out as described.[17] For RNase T1 structure mapping, radiolabeled RNA was incubated with 2.5 nM RNase T1 (Roche) for 20 minutes at 25 °C in buffer conditions identical with those used for X-ray scattering or under denaturing conditions,[48] and analyzed as in hydroxyl radical footprinting reactions.

Acknowledgements

We thank K. Travers for insightful and helpful discussion; K. Ito for expert user support and for use of unpublished CCD software at the Photon Factory through an agreement with the Stanford Synchrotron Radiation Laboratory (supported by NIH and DOE); and S. Seifert at the Advanced Photon Source (DOE contract no. W-31-109-Eng-38). This work was supported by NIH grants R01-GM-52348, P01-GM-66275 and an NSF fellowship (to R.D.).

Supplementary data

Supplementary data associated with this article can be found, in the online version, at doi:10.1016/j.jmb.2004.08.080

References

1. Joyce, G. F. & Orgel, L. E. (1993). Prospects for understanding the origin of the RNA world. In *The RNA World* (Atkins, J. F., ed), Cold Spring Harbor Laboratory Press, Cold Spring Harbor, NY, pp. 1–25.
2. Brion, P. & Westhof, E. (1997). Hierarchy and dynamics of RNA folding. *Annu. Rev. Biophys. Biomol. Struct.* **26**, 113–137.
3. Yoshida, A., Shan, S., Herschlag, D. & Piccirilli, J. A. (2000). The role of the cleavage site 2′-hydroxyl in the *Tetrahymena* group I ribozyme reaction. *Chem. Biol.* **7**, 85–96.
4. Rupert, P. B. & Ferre-D'Amare, A. R. (2001). Crystal structure of a hairpin ribozyme–inhibitor complex with implications for catalysis. *Nature*, **410**, 780–786.
5. Li, Y. & Breaker, R. R. (1999). Deoxyribozymes: new players in the ancient game of biocatalysis. *Curr. Opin. Struct. Biol.* **9**, 315–323.
6. Paquette, J., Nicoghosian, K., Qi, G. R., Beauchemin, N. & Cedergren, R. (1990). The conformation of single-stranded nucleic acids tDNA *versus* tRNA. *Eur. J. Biochem.* **189**, 259–265.
7. Pan, T., Long, D. M. & Uhlenbeck, O. C. (1993). Divalent metal ions in RNA dolding and catalysis. In *The RNA World* (Atkins, J. F., ed), Cold Spring Harbor Laboratory Press, Cold Spring Harbor, NY, pp. 271–302.
8. Yarus, M. (1993). How many catalytic RNAs? Ions and the Cheshire cat conjecture. *FASEB J.* **7**, 31–39.
9. Murray, J. B., Seyhan, A. A., Walter, N. G., Burke, J. M. & Scott, W. G. (1998). The hammerhead, hairpin and VS ribozymes are catalytically proficient in monovalent cations alone. *Chem. Biol.* **5**, 587–595.
10. Shelton, V. M., Sosnick, T. R. & Pan, T. (2001). Altering the intermediate in the equilibrium folding of unmodified yeast $tRNA^{Phe}$ with monovalent and divalent cations. *Biochemistry*, **40**, 3629–3638.
11. O'Rear, J. L., Wang, S., Feig, A. L., Beigelman, L., Uhlenbeck, O. C. & Herschlag, D. (2001). Comparison of the hammerhead cleavage reactions stimulated by monovalent and divalent cations. *RNA*, **7**, 537–545.
12. Takamoto, K., He, Q., Morris, S., Chance, M. R. & Brenowitz, M. (2002). Monovalent cations mediate formation of native tertiary structure of the *Tetrahymena thermophila* ribozyme. *Nature Struct. Biol.* **9**, 928–933.
13. Rangan, P. & Woodson, S. A. (2003). Structural requirement for Mg^{2+} binding in the group I intron core. *J. Mol. Biol.* **329**, 229–238.
14. Nesbitt, S., Hegg, L. A. & Fedor, M. J. (1997). An unusual pH-independent and metal-ion-independent mechanism for hairpin ribozyme catalysis. *Chem. Biol.* **4**, 619–630.
15. Suga, H., Cowan, J. A. & Szostak, J. W. (1998). Unusual metal ion catalysis in an acyl-transferase ribozyme. *Biochemistry*, **37**, 10118–10125.
16. Hertel, K. J., Peracchi, A., Uhlenbeck, O. C. & Herschlag, D. (1997). Use of intrinsic binding energy for catalysis by an RNA enzyme. *Proc. Natl Acad. Sci. USA*, **94**, 8497–8502.
17. Russell, R., Zhuang, X., Babcock, H. P., Millett, I. S., Doniach, S., Chu, S. & Herschlag, D. (2002). Exploring the folding landscape of a structured RNA. *Proc. Natl Acad. Sci. USA*, **99**, 155–160.
18. Cate, J. H., Gooding, A. R., Podell, E., Zhou, K., Golden, B. L., Kundrot, C. E. *et al*. (1996). Crystal structure of a group I ribozyme domain: principles of RNA packing. *Science*, **273**, 1678–1685.
19. Cate, J. H., Hanna, R. L. & Doudna, J. A. (1997). A magnesium ion core at the heart of a ribozyme domain. *Nature Struct. Biol.* **4**, 553–558.
20. Murphy, F. L. & Cech, T. R. (1993). An

independently folding domain of RNA tertiary structure within the *Tetrahymena* ribozyme. *Biochemistry*, **32**, 5291–5300.
21. Deras, M. L., Brenowitz, M., Ralston, C. Y., Chance, M. R. & Woodson, S. A. (2000). Folding mechanism of the *Tetrahymena* ribozyme P4-P6 domain. *Biochemistry*, **39**, 10975–11085.
22. Silverman, S. K., Deras, M. L., Woodson, S. A., Scaringe, S. A. & Cech, T. R. (2000). Multiple folding pathways for the P4-P6 RNA domain. *Biochemistry*, **39**, 12465–12475.
23. Uchida, T., He, Q., Ralston, C. Y., Brenowitz, M. & Chance, M. R. (2002). Linkage of monovalent and divalent ion binding in the folding of the P4-P6 domain of the *Tetrahymena thermophila* ribozyme. *Biochemistry*, **41**, 5799–5806.
24. Jaeger, J. A., Zuker, M. & Turner, D. H. (1990). Melting and chemical modification of a cyclized self-splicing group I intron: similarity of structures in 1 M Na^+, in 10 mM Mg^{2+}, and in the presence of substrate. *Biochemistry*, **29**, 10147–10158.
25. Draper, D. E. (2004). A guide to ions and RNA structure. *RNA*, **10**, 335–343.
26. Fang, X. W., Thiyagarajan, P., Sosnick, T. R. & Pan, T. (2002). The rate-limiting step in the folding of a large ribozyme without kinetic traps. *Proc. Natl Acad. Sci. USA*, **99**, 8518–8523.
27. Rangan, P., Masquida, B., Westhof, E. & Woodson, S. A. (2003). Assembly of core helices and rapid tertiary folding of a small bacterial group I ribozyme. *Proc. Natl Acad. Sci. USA*, **100**, 1574–1579.
28. Perez-Salas, U. A., Rangan, P., Krueger, S., Briber, R. M., Thirumalai, D. & Woodson, S. A. (2004). Compaction of a bacterial group I ribozyme coincides with the assembly of core helices. *Biochemistry*, **43**, 1746–1753.
29. Buchmueller, K. L. & Weeks, K. M. (2003). Near native structure in an RNA collapsed state. *Biochemistry*, **42**, 13869–13878.
30. Fang, X., Pan, T. & Sosnick, T. R. (1999). A thermodynamic framework and cooperativity in the tertiary folding of a Mg^{2+}-dependent ribozyme. *Biochemistry*, **38**, 16840–16846.
31. Chamberlin, S. I. & Weeks, K. M. (2003). Differential helix stabilities and sites pre-organized for tertiary interactions revealed by monitoring local nucleotide flexibility in the bI5 group I intron RNA. *Biochemistry*, **42**, 901–909.
32. Narlikar, G. J., Bartley, L. E. & Herschlag, D. (2000). Use of duplex rigidity for stability and specificity in RNA tertiary structure. *Biochemistry*, **39**, 6183–6189.
33. Das, R., Kwok, L. W., Millett, I., Bai, Y., Mills, T. T., Jacob, J. *et al*. (2003). The fastest global events in RNA folding: electrostatic relaxation and tertiary collapse of the *Tetrahymena* ribozyme. *J. Mol. Biol.* **332**, 311–319.
34. Murthy, V. L. & Rose, G. D. (2000). Is counterion delocalization responsible for collapse in RNA folding? *Biochemistry*, **39**, 14365–14370.
35. Bloomfield, V. A. (1997). DNA condensation by multivalent cations. *Biopolymers*, **44**, 269–282.
36. Basu, S., Rambo, R. P., Strauss-Soukup, J., Cate, J. H., Ferre-D'Amare, A. R., Strobel, S. A. & Doudna, J. A. (1998). A specific monovalent metal ion integral to the AA platform of the RNA tetraloop receptor. *Nature Struct. Biol.* **5**, 986–992.
37. Conn, G. L., Gittis, A. G., Lattman, E. E., Misra, V. K. & Draper, D. E. (2002). A compact RNA tertiary structure contains a buried backbone–K^+ complex. *J. Mol. Biol.* **318**, 963–973.
38. Hohng, S., Wilson, T. J., Tan, E., Clegg, R. M., Lilley, D. M. & Ha, T. (2004). Conformational flexibility of four-way junctions in RNA. *J. Mol. Biol.* **336**, 69–79.
39. Lilley, D. M. (2000). Structures of helical junctions in nucleic acids. *Quart. Rev. Biophys.* **33**, 109–159.
40. Szewczak, A. A. & Cech, T. R. (1997). An RNA internal loop acts as a hinge to facilitate ribozyme folding and catalysis. *RNA*, **3**, 838–849.
41. Uchida, T., Takamoto, K., He, Q., Chance, M. R. & Brenowitz, M. (2003). Multiple monovalent ion-dependent pathways for the folding of the L-21 *Tetrahymena thermophila* ribozyme. *J. Mol. Biol.* **328**, 463–478.
42. Seifert, S., Winans, R. E., Tiede, D. M. & Thiyagarajan, P. (2000). Design and performance of a ASAXS instrument at the advanced photon source. *J. Appl. Crystallog.* **33**, 782–784.
43. Amemiya, Y., Wakabayashi, K., Hamanaka, T., Wakabayashi, T., Matsushita, T. & Hashizume, H. (1983). Design of a small-angle diffractometer using synchrotron radiation at the photon factory. *Nucl. Instrum. Methods*, **208**, 471–477.
44. Svergun, D. I. (1992). Determination of the regularization parameter in indirect-transform methods using perceptual criteria. *J. Appl. Crystallog.* **25**, 495–503.
45. Skibinska, L., Gapinski, J., Liu, H., Patkowski, A., Fischer, E. W. & Pecora, R. (1999). Effect of electrostatic interactions on the structure and dynamics of a model polyelectrolyte. II. Intermolecular correlations. *J. Chem. Phys.* **110**, 1794–1800.
46. Das, R., Mills, T. T., Kwok, L. W., Maskel, G. S., Millett, I. S., Doniach, S. *et al*. (2003). Counterion distribution around DNA probed by solution X-ray scattering. *Phys. Rev. Letters*, **90**, 188103.
47. Wu, M. & Tinoco, I. J. (1999). RNA folding causes secondary structure rearrangement. *RNA*, **5**, 1665–1674.
48. Donis-Keller, H., Maxam, A. M. & Gilbert, W. (1977). Mapping adenines, guanines, and pyrimidines in RNA. *Nucl. Acids Res.* **4**, 2527–2538.
49. Silverman, S. K., Zheng, M., Wu, M., Tinoco, I., Jr & Cech, T. R. (1999). Quantifying the energetic interplay of RNA tertiary and secondary structure interactions. *RNA*, **5**, 1665–1674.
50. Takamoto, K., Chance, M. R. & Brenowitz, M. (2004). Semi-automated, single-band peak-fitting analysis of hydroxyl radical nucleic acid footprint autoradiograms for the quantitative analysis of transitions. *Nucl. Acids Res.* **32**, E119.
51. Heilman-Miller, S. L., Thirumalai, D. & Woodson, S. A. (2001). Role of counterion condensation in folding of the *Tetrahymena* ribozyme. I. Equilibrium stabilization by cations. *J. Mol. Biol.* **306**, 1157–1166.
52. Lee, N. & Thirumalai, D. (2000). Dynamics of collapse of flexible polyampholytes. *J. Chem. Phys.* **113**, 5126.
53. Mikulecky, P. J. & Feig, A. L. (2004). Heat capacity changes in RNA folding: application of perturbation theory to hammerhead ribozyme cold denaturation. *Nucl. Acids Res.* **32**, 3967–3976.
54. Rueda, D., Wick, K., McDowell, S. E. & Walter, N. G. (2003). Diffusely bound Mg^{2+} ions slightly reorient stems I and II of the hammerhead ribozyme to increase the probability of formation of the catalytic core. *Biochemistry*, **42**, 9924–9936.

55. Friederich, M. W., Vacano, E. & Hagerman, P. J. (1998). Global flexibility of tertiary structure in RNA: yeast $tRNA^{Phe}$ as a model system. *Proc. Natl. Acad. Sci. USA.* **95**, 3572–3577.
56. Lehnert, V., Jaeger, L., Michel, F. & Westhof, E. (1996). New loop–loop tertiary interactions in self-splicing introns of subgroup IC and ID: a complete 3D model of the *Tetrahymena thermophila* ribozyme. *Chem. Biol.* **3**, 993–1009.
57. Russell, R., Millett, I. S., Doniach, S. & Herschlag, D. (2000). Small angle X-ray scattering reveals a compact intermediate in RNA folding. *Nat. Struct. Biol.* **7**, 367–370.

Edited by J. Doudna

(Received 15 July 2004; received in revised form 24 August 2004; accepted 26 August 2004)